RSC Applied Polymers

ROYAL SOCIETY OF CHEMISTRY

PAPER

View Article Online
View Journal | View Issue

Check for updates

Cite this: *RSC Appl. Polym.*, 2026, **4**, 716

Chloroform outperforms chlorobenzene for enhanced mobility in amphiphilic polymer OFETs

Preeti Yadav,[a] Shunsuke Yamamoto,[b,c] Kodai Yamanaka,[d] Hengyuan Wang,[e] Nadège Bonnet,[a] Yabing Qi,[e] Itaru Osaka[d] and Christine K. Luscombe[*a]

High carrier mobility in conjugated polymer-based organic field-effect transistors (OFETs) is often achieved in polymer thin films that display well-ordered long-range structures and good intercrystallite connectivity. While chlorobenzene (CB) is commonly known to yield favorable morphologies for efficient charge transport, in this work, we demonstrate enhanced mobility in the case of chloroform (CF)-processed films over CB. We find that OFETs fabricated from CF exhibit an average mobility of 5.1×10^{-3} cm^2 V^{-1} s^{-1}, showing nearly a two-fold increase compared to the 2.7×10^{-3} cm^2 V^{-1} s^{-1} achieved by the CB protocol. A detailed study of the polymer morphology through UV-vis spectroscopy, GIWAXS, and pMAIRS suggests that large crystallite size and uniform polymer orientation in both crystalline and amorphous domains for CF-processed films led to improved mobility despite the greater local electronic order and lower *g*-parameter observed in the CB-films. This superior performance observed in CF- over CB-processed films is hypothesized to be due to the amphiphilic nature of the polymer poly(3-hexyl-4′-((2-methoxyethoxy)methyl)-2,2′-bithiophene). Our findings open new avenues for the independent control of electronic order and macroscopic crystallinity through the design of an amphiphilic polymer.

Received 9th October 2025,
Accepted 18th January 2026

DOI: 10.1039/d5lp00320b

rsc.li/rscapplpolym

Open Access Article. Published on 20 January 2026. Downloaded on 6/13/2026 12:19:35 AM.
This article is licensed under a Creative Commons Attribution-NonCommercial 3.0 Unported Licence.

1. Introduction

Organic field-effect transistors (OFETs) based on conjugated polymers have attracted widespread attention for the development of next-generation electronic circuits.[1–3] The rich chemistry of conjugated polymers, solution processability, their compatibility with flexible substrates, and low-temperature fabrication methods offer great potential for enabling the development of technologies that are currently not accessible with traditional silicon-based transistors.[4–8] Progress in this field has been significant, with polymer-based OFETs currently being investigated for diverse applications in sensors,[3,9] artificial synapses,[10] memory devices[11,12] and frequency identification tags.[13]

Charge carrier mobility is the key performance metric of OFETs, and considerable efforts have been devoted to enhancing it. Significant advances in both the molecular design of conjugated polymers and device engineering have remarkably improved the carrier mobilities from the very low values of 10^{-5} cm^2 V^{-1} s^{-1} observed in early polythiophene studies[14] to ≥1–10 cm^2 V^{-1} s^{-1} in a number of polymers.[15–20] Despite these great efforts, carrier mobility values of conjugated polymers still lag behind those of crystalline silicon-based semiconductors.

Detailed experimental studies have revealed that charge carrier transport is significantly affected by polymer film morphologies.[21–26] High mobility is typically associated with large crystallite size, long-range order, strong π–π stacking, low paracrystalline disorder (*g*), and greater electronic order. Furthermore, charge carrier transport hinges on good intercrystallite connectivity, particularly across the amorphous regions, and high backbone planarity. Ideally, the distance between the crystal domains should be less than the persistence length (l_p), and the polymer chains should maintain coplanarity as they traverse crystalline–amorphous interfaces.[27–31] Some recent studies have highlighted that local segmental order is enough for efficient charge transport based on good intercrystallite connectivity, regardless of crystallinity.[32] Very often, these structural features are achieved by using non-volatile solvents such as CB, as longer evaporation time facilitates the self-assembly of polymer chains into well-ordered structures, with larger grain size.[33–35] However, the use of volatile solvents is more beneficial from a fabrica-

[a]*Pi-conjugated polymers unit, Okinawa Institute of Science and Technology Graduate University, 1919-1 Tancha, Onna-son, Kunigami-gun, Okinawa, 904-0495, Japan. E-mail: christine.luscombe@oist.jp*
[b]*Graduate School of Engineering, Tohoku University, 6-6-11 Aramaki Aza Aoba, Aoba-ku, Sendai 980-8579, Japan*
[c]*Graduate School of Engineering, Kyoto University, Katsura, Nishikyo-ku, Kyoto 615-8510, Japan*
[d]*Graduate School of Advanced Science and Engineering, Hiroshima University, 1-4-1 Kagamiyama, Higashi-Hiroshima, Hiroshima, 739-8527, Japan*
[e]*Energy Materials and Surface Sciences Unit (EMSSU), Okinawa Institute of Science and Technology Graduate University, 1919-1 Tancha, Onna-son, Kunigami-gun, Okinawa 904-0495, Japan*

© 2026 The Author(s). Published by the Royal Society of Chemistry

Open Access Article. Published on 20 January 2026. Downloaded on 6/13/2026 12:19:35 AM. This article is licensed under a Creative Commons Attribution-NonCommercial 3.0 Unported Licence.

tion point of view. Though the faster drying kinetics of low volatile solvents seem more suitable from a manufacturing and scalability perspective, lower crystallinity resulting from poor polymer ordering often limits the charge carrier mobilities as demonstrated in previous studies.[33,36,37]

Contrary to previous paradigms, herein, we present a counter-intuitive case study where CF-processed OFET devices exhibit higher mobility compared to those processed using CB. To understand this, we performed UV-visible absorption spectroscopy, *p*-polarized multiple-angle incidence resolution spectrometry (pMAIRS), and grazing incidence wide-angle X-ray scattering (GIWAXS) and found that even though CB shows greater local electronic order and lower paracrystallinity, a two-fold increase in field-effect mobility in CF, resulting from large crystallite size and uniform polymer orientation, is observed despite its more amorphous nature. We attribute this unexpected behaviour to the amphiphilic nature of the polymer. In this work, we aim to deconstruct the trade-off of all the competing factors that affect charge mobility by using an amphiphilic polymer poly(3-hexyl-4′-((2-methoxyethoxy)methyl)-2,2′-bithiophene) (P3HMEMT) (Fig. 1a) comprising ethylene glycol and alkyl side chains. We chose P3HMEMT as a model system because of its similarity to poly(3-hexylthiophene) (P3HT), which is a workhorse polymer in organic electronics, and low synthetic complexity. Furthermore, we envisaged that a perfectly alternating copolymer architecture with precise placements of polar oligoethylene glycol side chains on one side of the polymer backbone and non-polar hexyl side chains on the other would provide a versatile scaffold for investigating solution state aggregation and the resulting solid-state microstructure, and thus the charge transport properties.

2. Results

2.1 Enhancement of device performance *via* solvent protocol

Bottom-gate (Si) top-contact configuration OFETs with variable length and width ratios were fabricated to investigate the charge mobility of the polymer P3HMEMT. All polymer films were thermally annealed at 130 °C for 30 minutes under vacuum. These conditions were chosen to ensure complete solvent removal and allow for polymer relaxation, consistent with processing windows of P3HT-based analogs. The synthesis of P3HMEMT and the device fabrication details are provided in the SI. Fig. 1c–f shows the transfer and output curves of the OFET devices fabricated from CF and CB. Both CF and CB films exhibit typical linear/saturation behaviour in their transfer and output characteristics. Charge mobilities were extracted from the linear region of the transfer curves and summarized in Table S1. OFETs fabricated using the CF protocol exhibited an average charge mobility of 5.1×10^{-3} cm^2 V^{-1} s^{-1}, demonstrating a two-fold increase relative to the 2.7×10^{-3} cm^2 V^{-1} s^{-1} achieved with the CB protocol. Interestingly, this observation contrasts significantly with other conjugated polymers including P3HT, where CB is consistently shown to provide greater mobility.[33–37]

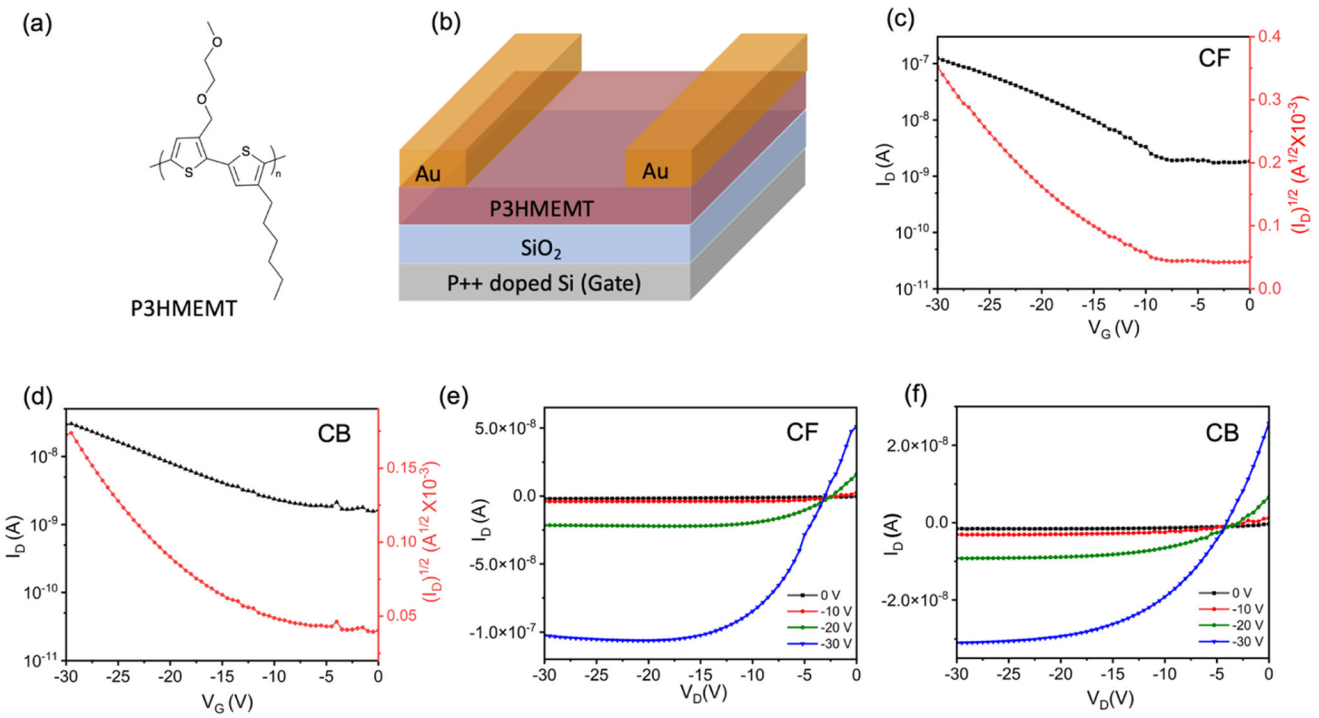

Fig. 1 (a) Chemical structure of the polymer P3HMEMT, (b) OFET device configuration, (c and d) transfer, and (e and f) output characteristics for OFET devices fabricated from CF and CB solvent with channel width of 152 μm, and length of 44 μm.

Open Access Article. Published on 20 January 2026. Downloaded on 6/13/2026 12:19:35 AM. This article is licensed under a Creative Commons Attribution-NonCommercial 3.0 Unported Licence.

2.2 Analysis of local electronic order

Fig. 2 shows the UV-vis absorption spectra of thin films fabricated from CF and CB. The UV-vis spectrum of the CF-film exhibited an absorption maximum at 514 nm and a very weak vibronic or shoulder peak at 590 nm. In contrast, the CB-film spectrum is red-shifted showing an absorption maximum at 545 nm and two distinct shoulder peaks around 522 nm and 590 nm. The observation of well-resolved vibronic peaks in the CB-film reflects an ordered planar chain conformation, indicative of enhanced local order compared to the CF protocol. It is noteworthy that there is more amorphous content in the CF-film, indicated by greater absorption in the region <500 nm, which is consistent with existing literature trends.[35,36]

2.3 Resulting macroscopic film morphology

To gain insight into how the structural arrangement of the polymer backbone and side chains in P3HMEMT governs the packing and conformational arrangement, we employed pMAIRS to probe the molecular arrangement of the whole film.

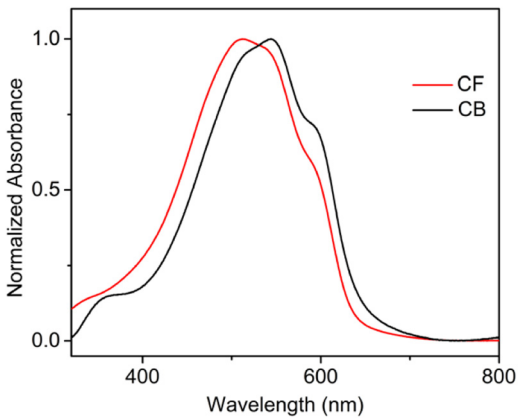

Fig. 2 Normalized UV-vis absorption spectra of CF- and CB-processed thin films.

Fig. 3 shows the IR-pMAIRS spectra of P3HMEMT films prepared using the CF and CB protocols. The red line and blue line correspond to in-plane (IP) and out-of-plane (OP) spectra, respectively. These spectra reveal four distinct absorption bands at around 2800, 1510, 1100, and 820 cm^{-1}. In previous studies on poly(alkylthiophenes),[38] two bands at *ca.* 1510 and 820 cm^{-1} are assigned to the ring antisymmetric stretching vibration (ν(C=C)) and the C–H out-of-plane deformation vibration (γ(C–H)) modes of the thiophene rings, respectively. The high-wavenumber region is ascribed to C–H vibrations (ν(C–H)) of alkyl and ethylene oxide side chains. A strong peak signal appears at 2926 cm^{-1} for both CF and CB samples, which is attributed to the antisymmetric C–H vibrations (ν_{as}(C–H)) of alkyl chains with Gauche-rich conformers,[39,40] showing similar intensity in both the IP and OP spectra. This means alkyl side chains in both CF and CB samples assume random orientation and Gauche-rich conformation. Ethylene glycol side chains have distinct vibrational modes derived from C–O vibrations found in regions at 1100 and 850 cm^{-1} (see the SI for details): antisymmetric stretching vibrations ν(C–O) at *ca.* 1100 and 1120 cm^{-1} from the side chain end and the side chain root ν_2 of ethylene glycol side chains,[41] and the rocking vibration ($\rho(CH_2)$) mode of the *gauche* conformer of the ethylene glycol side chains at *ca.* 850 cm^{-1}. Based on these peak assignments, we will focus on the three regions shown in Fig. 3(b). In the thiophene ν(C=C) bands at 1510 cm^{-1}, stronger absorption in the IP spectra than in the OP spectra, is indicative of anisotropic alignment of polymer chains. Given the transition moment of this vibration orients to the long-axis of polymer chains, the main chains lie on the substrate surface in all films. The order parameter $\langle S \rangle$ can be estimated for more detailed analysis as summarized in Table 1:[42]

$$\langle S \rangle = \frac{A_{OP} - A_{IP}}{A_{OP} + 2A_{IP}} = \frac{1}{2}(3\langle \cos^2 \theta \rangle - 1) \quad (1)$$

The CF and CB polymer films show similar values of $\langle S \rangle$, suggesting similar orientation of main chains regardless of spin-coating solvent. The orientation of the thiophene rings is

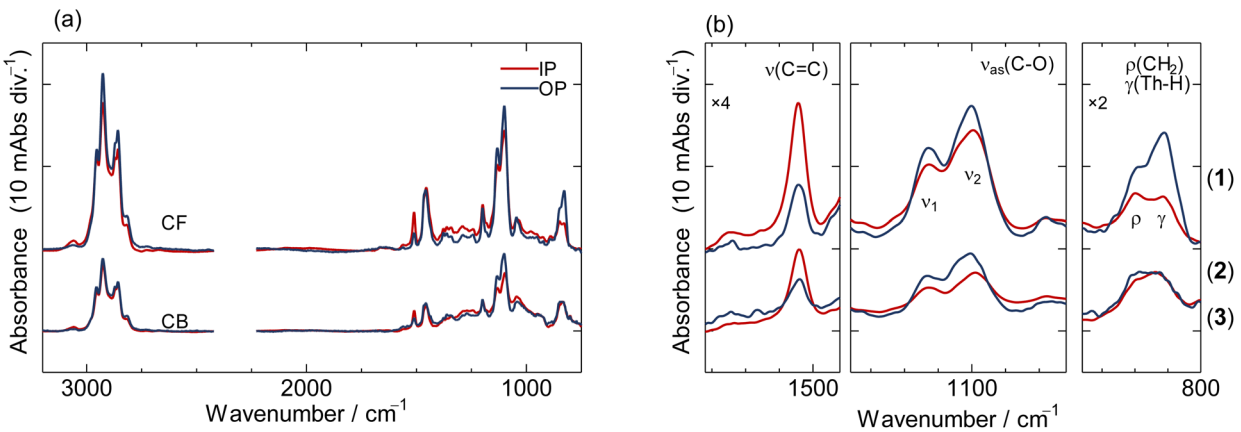

Fig. 3 pMAIRS spectra of CF- and CB-processed films. The red and blue lines correspond to IP and OP spectra: (a) all wavenumber range, and (b) magnified spectra at representative modes.

© 2026 The Author(s). Published by the Royal Society of Chemistry

Open Access Article. Published on 20 January 2026. Downloaded on 6/13/2026 12:19:35 AM. This article is licensed under a Creative Commons Attribution-NonCommercial 3.0 Unported Licence.

Table 1 Order parameters $\langle S \rangle$ of each vibration mode estimated from the pMAIRS spectra shown in Fig. 3

Sample type	ν(C=C)	γ(C–H)	ν(C–O) end-side ν_1	ν(C–O) root-side ν_2
CF	−0.23	0.37	0.11	0.09
CB	−0.21	−0.04	0.16	0.15

determined from the γ(C–H) peaks. This mode has a perpendicular transition moment to the thiophene ring, and therefore a positive $\langle S \rangle$ value indicates face-on orientation. The $\langle S \rangle$ values of the γ(C–H) peaks were estimated from peak deconvolution (see the SI for details) of the adjacent $\rho(CH_2)$ mode. As a result, the CF film shows $\langle S \rangle$ values around 0.37, while the CB sample shows almost zero value. These results indicate the face-on orientation of thiophene rings for CF, while CB assumes a nearly random thiophene orientation as a whole.

The bimodal ν(C–O) peaks from ethylene glycol side chains of different positions (end-side and root-side) show a similar intensity ratio between IP and OP. For both the CF and CB samples, the $\langle S \rangle$ values of ν_1 and ν_2 are nearly the same, but slightly larger values for the end side indicate that glycol side chains are randomly oriented with almost straight conformation, while alkyl side chains assume the Gauche conformation with random orientation. Table 2 summarizes the molecular orientations of each moiety from the pMAIRS analysis. The polymer film from CB, which requires a longer time to dry during the film formation process, has more ordered ethylene glycol side chains than that from CF, whereas the ordering of the backbone is poorer. We note that this is consistent with our observation from GIWAXS data for CB (discussed in the next section), which shows a mixed π-face and edge-on lamellar orientation along with smaller crystallite size, but stands in contrast to UV-vis studies that indicate greater backbone planarity. Given that pMAIRS includes the contribution of amorphous domains and aggregates that are not detectable by GIWAXS, it therefore provides details on the amorphous domain, and hence polymer orientation in the intercrystallite region, as well.

2.4 Crystallinity analysis by GIWAXS

Having examined the morphologies of the entire film, we now take a closer look at the molecular packing and orientation within the crystalline domains. We performed GIWAXS to determine the material crystallinity, molecular stacking, and orientation in both films. Fig. 4 shows the two-dimensional (2D) GIWAXS patterns and corresponding line-cut profiles in the in-plane (q_{xy}) and out-of-plane (q_z) directions and the relevant packing parameters, including stacking distance, crystallite size, and paracrystallinity (characterized by the g-parameter), all of which are listed in Table 3.

As depicted in Fig. 4, the CF-film exhibits a strong lamellar stacking (100) peak in the in-plane direction and (010) π–π stacking peak in the out-of-plane direction, indicative of a uniform face-on orientation adopted by the crystallites. Furthermore, higher-order lamellar peaks are observed indicating long-range crystallite order. Interestingly, the CB-film shows a completely different GIWAXS pattern: the weaker intensity of the (100) peak in the in-plane direction, while the more pronounced intensity in the out-of-plane direction indicates mixed/random orientation adopted by the π-face although lamella peaks indicate edge-on conformation. This suggests a layered structure adopted in the CB-film; however, the π-face is randomly oriented between the crystals. The lamellar spacing and π–π stacking distance of the CF-film were found to be 15.7 and 3.7 Å, comparable to the values of 15.6 and 3.7 Å, respectively, in the CB-film. However, there is a significant difference in the crystallite sizes. The crystallite coherence lengths for lamellar and π–π stacking structures were estimated to be 252 and 42 Å for the CF-film, much higher than 101 and 29 Å in the case of the CB-film, suggesting larger crystalline domains in CF. Interestingly, this trend appears to be in contrast to other polymer systems where CB typically promotes large crystalline domains and enhanced order.[34,36] We also calculated the g-parameter associated with lamellar and π–π stacking structures.[43] A decrease in g-parameter for both the π–π stacking and lamellar stacking structures for CB is indicative of slightly fewer defects compared to the CF film corroborating the seemingly contradictory UV-vis data. Overall, the above results provide an indication that the improved OFET mobility of the CF film results from its large crystallite size and uniform polymer orientation in both the amorphous and crystalline domains despite the greater amorphous content.

3. Discussion

Based on the characterization results, the improved OFET performance in the CF films compared to the CB films can be explained by considering the factors described in the following sections.

Table 2 Molecular orientation estimated from Fig. 3 and Table 1

Sample type	Main chain	Thiophene rings	Ethylene glycol side chains	Alkyl side chains
CF	Parallel to the substrate	Face-on	Conformation: almost straight Orientation: random	Conformation: gauche Orientation: random
CB	Parallel to the substrate	Coplanar in segment level, but random in total	Conformation: almost straight Orientation: random	Conformation: gauche Orientation: random

© 2026 The Author(s). Published by the Royal Society of Chemistry

Open Access Article. Published on 20 January 2026. Downloaded on 6/13/2026 12:19:35 AM.
This article is licensed under a Creative Commons Attribution-NonCommercial 3.0 Unported Licence.

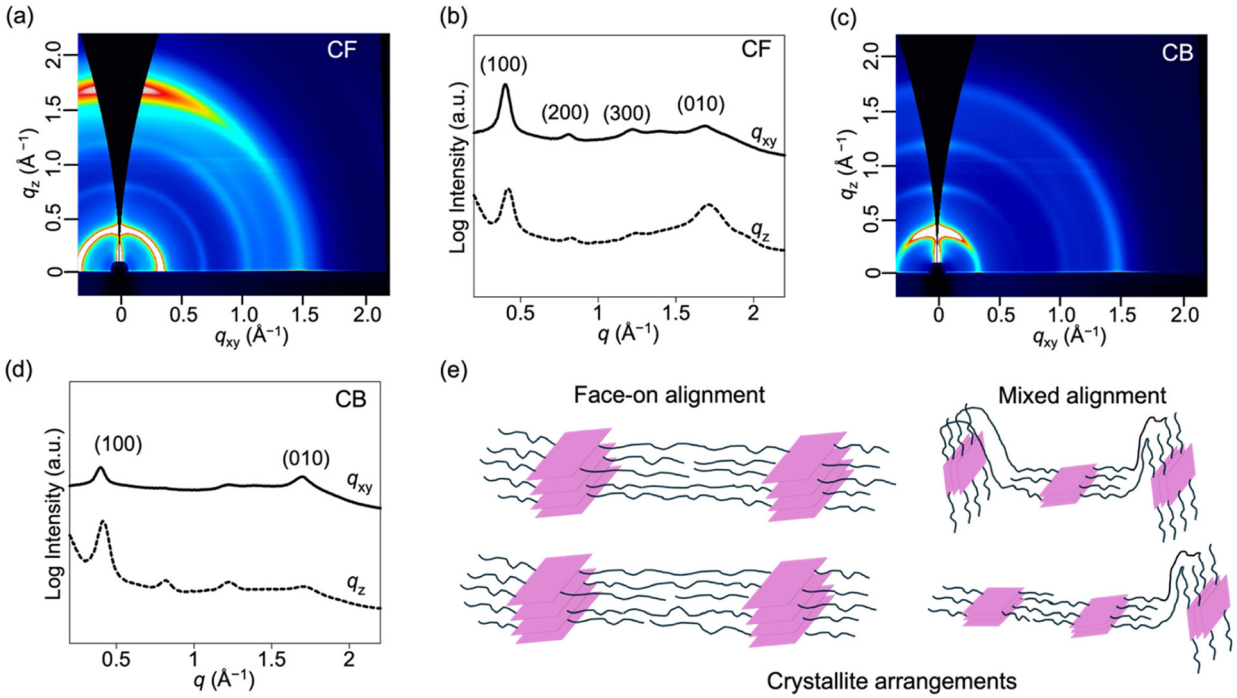

Fig. 4 2D-GIWAXS patterns (a, c) and the corresponding line-cut profile (b, d) and a schematic representation of crystallite arrangements of thin films fabricated from CF (e) and CB (f), respectively.

Table 3 Parameters obtained from GIWAXS measurement of P3HMEMT thin films prepared from CF and CB

					Face-on[e]		Edge-on[f]	
Sample type	d_L[a] (Å)	L_L[b] (Å)	d_π[c] (Å)	L_π[d] (Å)	$g_{F,100}$	$g_{F,010}$	$g_{E,100}$	$g_{E,010}$
CF	15.7	252	3.68	42	14.1	12.8	15.8	15.1
CB	15.6	101	3.66	29	15.7	10.2	15.7	11.3

[a] d-Spacing for lamellar structure. [b] Crystallite coherence length for lamellar structure. [c] d-Spacing for π–π stacking structure. [d] Crystallite coherence length for π–π stacking structure. [e] $g_{F,100}$ and $g_{F,010}$ corresponds to paracrystalline disorder along the lamellar and π–π stacking directions of face-on crystallites. [f] $g_{E,100}$ and $g_{E,010}$ corresponds to paracrystalline disorder along the lamellar and π–π stacking directions of edge-on crystallites.

3.1 The competing factors

The CB protocol leads to a seemingly favourable microstructure for efficient charge transport, exhibiting high local electronic order, lower g-parameter, and mixed orientation of the polymer crystal (previous studies have shown that for in-plane mobility, edge-on packing is the most favourable, followed by mixed and face-on[37]). Although GIWAXS analysis suggests reduced macroscopic crystallinity, UV-vis studies indicate a smaller amorphous fraction in the CB film. On the other hand, the CF protocol is favoured for yielding large crystallite domains and uniform polymer orientation. Because intercrystallite hopping is reported to be the limiting factor for charge transport,[44] greater mobility observed for the CF film likely arises from either physical connectivity through tie chains or electronic connectivity, in addition to the larger crystals, leading to the observed enhancement in charge transport properties. Notably, pMAIRS analysis supports this rationale since the thiophene rings in the CF-processed film exhibit uniform face-on orientation, whereas CB leads to a film with random/mixed orientation of the thiophene rings. Based on this, we hypothesize that crystallite orientation dictates the intercrystallite connectivity and performance in CF-processed films. Although the crystal microstructure is more disordered, it is the film's connectivity that determines the performance.

3.2 Linking polymer chemistry to conformation control

With hydrophobic polymers, CB leads to greater performance, resulting from the formation of more-ordered thin films. However, the performance improvement in CF-processed film over CB-processed film, contrary to typical trends, is hypothesized to originate from the amphiphilic nature of the polymer. We anticipate that CF, being relatively less hydrophobic than CB, does not exhibit any strong preference for either the hydrophilic or hydrophobic side chains. In contrast, CB would exhibit a strong preference for hydrophobic side chains due to its higher hydrophobicity, which could lead to

© 2026 The Author(s). Published by the Royal Society of Chemistry

Open Access Article. Published on 20 January 2026. Downloaded on 6/13/2026 12:19:35 AM.
This article is licensed under a Creative Commons Attribution-NonCommercial 3.0 Unported Licence.

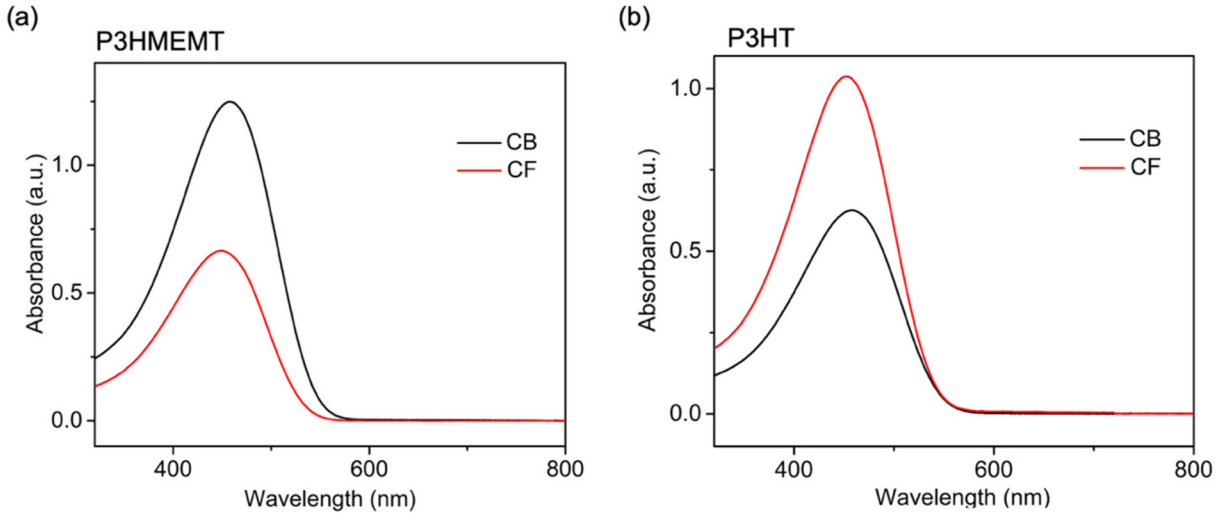

Fig. 5 UV-vis absorption spectra of (a) P3HMEMT and (b) P3HT in CF and CB solutions (0.015 mg mL^{-1}).

the formation of micelle-like structures.[45–47] These micelle-like structures may interfere with polymer self-assembly, thereby affecting the crystal growth and limiting the crystallite size. However, since CB is less volatile, the resulting crystal structure likely exhibits fewer defects, consistent with the literature reports.[34–36,48] The solution UV-vis spectra provide some support for this hypothesis (Fig. 5). The solution spectrum of P3HMEMT in CB is red-shifted by 10 nm and shows an increase in intensity compared to the solution spectrum in CF. This suggests J-type aggregate behaviour. However, the CB peak also broadens compared to that of CF, suggesting that there is inhomogeneity. In contrast, the UV-vis spectrum of P3HT solution in CB is red-shifted by 6 nm and exhibits a decrease in peak intensity and a narrowing of the peak compared to CF. This implies more HJ-type mixed aggregate behavior and more homogeneous aggregates. The combination of a red-shifted peak and spectral broadening for P3HMEMT suggests the formation of discrete, micelle-like structures. This implies that while the polymer chains achieve local order within each micelle, the overall solution becomes inhomogeneous due to the distribution of these aggregates, which can vary in size and shape. In contrast, the peak narrowing observed for the fully hydrophobic P3HT suggests it forms more homogeneous aggregates, pointing to more uniform, extended self-assembly. We emphasize that confirming the hypothesis is a subject of future study. While the observed differences in charge mobility and morphology could be rationalized by this working hypothesis, further experimental studies are required to validate it.

4. Conclusions

In this work, our investigation has focused on systematically deconstructing the complex interplay of molecular packing, crystalline order, and intercrystallite connectivity that governs the charge transport for achieving high-performance OFETs by using an amphiphilic copolymer. We demonstrated a significant improvement in OFET mobility in an amphiphilic copolymer P3HMEMT with CF as the processing solvent compared to CB, despite more favourable microstructure in CB-processed films. CB-processed film exhibited greater electronic order, lower *g*-parameter, and mixed orientation of the π-face while lamellae are randomly oriented, as evidenced from UV-vis, pMAIRS, and GIWAXS results. On the other hand, greater amorphous content, face-on orientation and larger crystallite domains are seen in CF-processed films. Benefitting from the large crystal size and uniform crystallite orientation, OFET devices fabricated from CF-processed film exhibited an average mobility of 5.1 × 10^{-3} cm^2 V^{-1} s^{-1}, a two-fold increase compared to the value of 2.7 × 10^{-3} cm^2 V^{-1} s^{-1} achieved by following the CB protocol. Future work will focus on leveraging the interplay of the amphiphilic polymer design and solvent to enable greater performance. While electronic order and macroscopic crystallinity are typically intertwined, this study provides other avenues to control each independently for the development of high-performance OFETs.

Author contributions

C. K. L. conceived the project and designed the experiments. P. Y. carried out the material synthesis and characterization, UV-vis spectroscopy measurements, participated in the device fabrication and characterization, and data analysis. S. Y. performed the pMAIRS measurements and analyzed the data. Y. K. and I. O. performed the GIWAXS measurements and analyzed the data. N. B. prepared the samples for GIWAXS measurements. H. W. and Y. Q. contributed to the OFET device fabrication and characterizations. P. Y., S. Y., and C. K. L. co-wrote the paper. All authors commented on the manuscript.

© 2026 The Author(s). Published by the Royal Society of Chemistry

Open Access Article. Published on 20 January 2026. Downloaded on 6/13/2026 12:19:35 AM. This article is licensed under a Creative Commons Attribution-NonCommercial 3.0 Unported Licence.

Conflicts of interest

There are no conflicts to declare.

Data availability

The data supporting this article have been included as part of the supplementary information (SI). Supplementary information: material synthesis and characterization studies, thin-film fabrication and characterization, peak assignments of IR spectra, OFET fabrication, and mobility data. See DOI: https://doi.org/10.1039/d5lp00320b.

Acknowledgements

Financial support from the Okinawa Institute of Science and Technology, and JSPS KAKENHI Grant Number JP24K08518. GIWAXS measurements were performed at BL13XU of SPring-8 with the approval of the Japan Synchrotron Radiation Research Institute (JASRI) (Proposal No. 2024A1666). The authors thank Dr T. Koganezawa (JASRI) for support in GIWAXS measurements.

References

1 H. Sirringhaus, P. J. Brown, R. H. Friend, M. M. Nielsen, K. Bechgaard, B. M. W. Langeveld-Voss, A. J. H. Spiering, R. A. J. Janssen, E. W. Meijer, P. Herwig and D. M. De Leeuw, Two-dimensional charge transport in self-organized, high-mobility conjugated polymers, *Nature*, 1999, **401**, 685–688.

2 I. McCulloch, M. Heeney, C. Bailey, K. Genevicius, I. MacDonald, M. Shkunov, D. Sparrowe, S. Tierney, R. Wagner, W. Zhang, M. L. Chabinyc, R. J. Kline, M. D. McGehee and M. F. Toney, Liquid-crystalline semiconducting polymers with high charge-carrier mobility, *Nat. Mater.*, 2006, **5**, 328–333.

3 S. Yuvaraja, A. Nawaz, Q. Liu, D. Dubal, S. G. Surya, K. N. Salama and P. Sonar, Organic field-effect transistor-based flexible sensors, *Chem. Soc. Rev.*, 2020, **49**, 3423–3460.

4 X. Guo, M. Baumgarten and K. Müllen, Designing π-conjugated polymers for organic electronics, *Prog. Polym. Sci.*, 2013, **38**, 1832–1908.

5 T. Nezakati, A. Seifalian, A. Tan and A. M. Seifalian, Conductive Polymers: Opportunities and Challenges in Biomedical Applications, *Chem. Rev.*, 2018, **118**, 6766–6843.

6 X. Guo and A. Facchetti, The journey of conducting polymers from discovery to application, *Nat. Mater.*, 2020, **19**, 922–928.

7 C. Wang, H. Dong, W. Hu, Y. Liu and D. Zhu, Semiconducting π-conjugated systems in field-effect transistors: A material odyssey of organic electronics, *Chem. Rev.*, 2012, **112**, 2208–2267.

8 T. M. Swager, 50th Anniversary Perspective: Conducting/Semiconducting Conjugated Polymers. A Personal Perspective on the Past and the Future, *Macromolecules*, 2017, **50**, 4867–4886.

9 W. Tang, Y. Fu, Y. Huang, Y. Li, Y. Song, X. Xi, Y. Yu, Y. Su, F. Yan and X. Guo, Solution processed low power organic field-effect transistor bio-chemical sensor of high transconductance efficiency, *npj Flexible Electron.*, 2022, **6**, 18.

10 B. Mandal, P. Sonar and S. P. Singh, Visible Light-Stimulated Artificial Synapse Based on an Organic Field-Effect Transistor for Imitating Human Emotions and Mood Swings, *ACS Appl. Electron. Mater.*, 2024, **6**, 2420–2433.

11 Y. C. Lin, C. C. Hung, C. K. Chen, Y. C. Chiang, L. C. Hsu, J. S. Li, C. C. Chueh, T. Higashihara and W. C. Chen, Pyrene-Incorporated Side Chain in π-Conjugated Polymers for Non-Volatile Transistor-Type Memory Devices with Improved Stretchability, *ACS Appl. Polym. Mater.*, 2021, **3**, 2109–2119.

12 Z. Zhu, Y. Guo and Y. Liu, Application of organic field-effect transistors in memory, *Mater. Chem. Front.*, 2020, **4**, 2845–2862.

13 R. Tinivella, V. Camarchia, M. Pirola, S. Shen and G. Ghione, Simulation and design of OFET RFIDs through an analog/digital physics-based library, *Org. Electron.*, 2011, **12**, 1328–1335.

14 A. Tsumura, H. Koezuka and T. Ando, Macromolecular electronic device: Field-effect transistor with a polythiophene thin film, *Appl. Phys. Lett.*, 1986, **49**, 1210–1212.

15 M. Makala, M. Barłóg, D. Dremann, S. Attar, E. G. Fernández, M. Al-Hashimi and O. D. Jurchescu, High-performance n-type polymer field-effect transistors with exceptional stability, *J. Mater. Chem. C*, 2024, **12**, 17089–17098.

16 N. Luo, P. Ren, Y. Feng, X. Shao, H. L. Zhang and Z. Liu, Side-Chain Engineering of Conjugated Polymers for High-Performance Organic Field-Effect Transistors, *J. Phys. Chem. Lett.*, 2022, **13**, 1131–1146.

17 M. Wang, G. Xia, C. Yang, L. Zhang, M. Nikolka, W. Zhang, C. Cendra, W. Liu, S. Zhao, J. Zeng, C. Zou, J. Gorenflot, A. Salleo, F. Laquai, H. Sirringhaus, I. McCulloch and H. Chen, An Amorphous Donor-Acceptor Conjugated Polymer with Both High Charge Carrier Mobility and Luminescence Quantum Efficiency, *Angew. Chem., Int. Ed.*, 2025, **64**, e202421199.

18 S. Sharma, A. K. Vats, L. Tang, F. Kaishan, J. Toyoda, S. Nagamatsu, Y. Ando, M. Tamagawa, H. Tanaka, M. Pandey and S. S. Pandey, High field-effect mobility in oriented thin films of D-A type semiconducting polymers by engineering stable interfacial system, *Chem. Eng. J.*, 2023, **469**, 143932.

19 M. Kim, S. U. Ryu, S. A. Park, K. Choi, T. Kim, D. Chung and T. Park, Donor–Acceptor-Conjugated Polymer for High-Performance Organic Field-Effect Transistors: A Progress Report, *Adv. Funct. Mater.*, 2020, **30**, 1904545.

20 X. Zhang, H. Bronstein, A. J. Kronemeijer, J. Smith, Y. Kim, R. J. Kline, L. J. Richter, T. D. Anthopoulos, H. Sirringhaus,

© 2026 The Author(s). Published by the Royal Society of Chemistry

Open Access Article. Published on 20 January 2026. Downloaded on 6/13/2026 12:19:35 AM. This article is licensed under a Creative Commons Attribution-NonCommercial 3.0 Unported Licence.

K. Song, M. Heeney, W. Zhang, I. McCulloch and D. M. Delongchamp, Molecular origin of high field-effect mobility in an indacenodithiophene- benzothiadiazole copolymer, *Nat. Commun.*, 2013, **4**, 2238.

21 K. Arlauskas, M. Viliu, K. Genevic, G. Jus and H. Stubb, Charge Transport in π-conjugated polymers, *Phys. Rev. B: Condens. Matter Mater. Phys.*, 2000, **62**, 235–238.

22 N. A. Kukhta and C. K. Luscombe, Gaining control over conjugated polymer morphology to improve the performance of organic electronics, *Chem. Commun.*, 2022, **58**, 6982–6997.

23 S. Y. Son, Y. Kim, J. Lee, G. Y. Lee, W. T. Park, Y. Y. Noh, C. E. Park and T. Park, High-Field-Effect Mobility of Low-Crystallinity Conjugated Polymers with Localized Aggregates, *J. Am. Chem. Soc.*, 2016, **138**, 8096–8103.

24 M. Nikolka, M. Hurhangee, A. Sadhanala, H. Chen, I. McCulloch and H. Sirringhaus, Correlation of Disorder and Charge Transport in a Range of Indacenodithiophene-Based Semiconducting Polymers, *Adv. Electron. Mater.*, 2018, **4**, 1700410.

25 N. Martino, D. Fazzi, C. Sciascia, A. Luzio, M. R. Antognazza and M. Caironi, Mapping orientational order of charge-probed domains in a semiconducting polymer, *ACS Nano*, 2014, **8**, 5968–5978.

26 T. Schuettfort, B. Watts, L. Thomsen, M. Lee, H. Sirringhaus and C. R. McNeill, Microstructure of polycrystalline PBTTT films: Domain mapping and structure formation, *ACS Nano*, 2012, **6**, 1849–1864.

27 S. Fratini, M. Nikolka, A. Salleo, G. Schweicher and H. Sirringhaus, Charge transport in high-mobility conjugated polymers and molecular semiconductors, *Nat. Mater.*, 2020, **19**, 491–450.

28 R. Noriega, J. Rivnay, K. Vandewal, F. P. V. Koch, N. Stingelin, P. Smith, M. F. Toney and A. Salleo, A general relationship between disorder, aggregation and charge transport in conjugated polymers, *Nat. Mater.*, 2013, **12**, 1038–1044.

29 P. Kohn, S. Huettner, H. Komber, V. Senkovskyy, R. Tkachov, A. Kiriy, R. H. Friend, U. Steiner, W. T. S. Huck, J. U. Sommer and M. Sommer, On the role of single regiodefects and polydispersity in regioregular poly(3-hexylthiophene): Defect distribution, synthesis of defect-free chains, and a simple model for the determination of crystallinity, *J. Am. Chem. Soc.*, 2012, **134**, 4790–4805.

30 D. Alberga, A. Perrier, I. Ciofini, G. F. Mangiatordi, G. Lattanzi and C. Adamo, Morphological and charge transport properties of amorphous and crystalline P3HT and PBTTT: Insights from theory, *Phys. Chem. Chem. Phys.*, 2015, **17**, 18742–18750.

31 A. Luzio, L. Criante, V. D'Innocenzo and M. Caironi, Control of charge transport in a semiconducting copolymer by solvent-induced long-range order, *Sci. Rep.*, 2013, **3**, 1–6.

32 S. Wang, S. Fabiano, S. Himmelberger, S. Puzinas, X. Crispin, A. Salleo and M. Berggren, Experimental evidence that short-range intermolecular aggregation is sufficient for efficient charge transport in conjugated polymers, *Proc. Natl. Acad. Sci. U. S. A.*, 2015, **112**, 10599–10604.

33 J. F. Chang, B. Sun, D. W. Breiby, M. M. Nielsen, T. I. Sölling, M. Giles, I. McCulloch and H. Sirringhaus, Enhanced Mobility of poly(3-hexylthiophene) transistors by spin-coating from high-boiling-point solvents, *Chem. Mater.*, 2004, **16**, 4772–4776.

34 K. Zhao, X. Yu, R. Li, A. Amassian and Y. Han, Solvent-dependent self-assembly and ordering in slow-drying drop-cast conjugated polymer films, *J. Mater. Chem. C*, 2015, **3**, 9842–9984.

35 X. Luo, L. Li, D. Li, Q. Zhao, H. Zhan, Y. Dong, Y. Han and J. Peng, Effect of Solution-State Aggregation on Solid-State Crystal Orientation in Donor-Acceptor Conjugated Copolymers, *Chem. Mater.*, 2024, **36**, 3726–3734.

36 P. K. H. Ho, L. L. Chua, M. Dipankar, X. Gao, D. Qi, A. T. S. Wee, J. F. Chang and R. H. Friend, Solvent effects on chain orientation and interchain π-interaction in conjugated polymer thin films: Direct measurements of the air and substrate interfaces by near-edge X-ray absorption spectroscopy, *Adv. Mater.*, 2007, **19**, 215–221.

37 B. C. Schroeder, T. Kurosawa, T. Fu, Y. C. Chiu, J. Mun, G. J. N. Wang, X. Gu, L. Shaw, J. W. E. Kneller, T. Kreouzis, M. F. Toney and Z. Bao, Taming Charge Transport in Semiconducting Polymers with Branched Alkyl Side Chains, *Adv. Funct. Mater.*, 2017, **27**, 17019.

38 N. Shioya, T. Shimoaka, K. Eda and T. Hasegawa, Controlling Mechanism of Molecular Orientation of Poly(3-alkylthiophene) in a Thin Film Revealed by Using pMAIRS, *Macromolecules*, 2017, **50**, 5090–5097.

39 R. A. Macphaiv, H. L. Strauss, R. G. Snyder and C. A. Elliger, C-H Stretching Modes and the Structure of n-Alkyl Chains. 2. Long, All-Trans Chains, *J. Phys. Chem.*, 1984, **88**, 334–341.

40 R. G. Snyder, H. L. Strauss and C. A. Elllger, C-H Stretching Modes and the Structure of n-Alkyl Chains. 1. Long, Disordered Chains, *J. Phys. Chem.*, 1982, **86**, 5145–5150.

41 T. Shimoaka and T. Hasegawa, Molecular structural analysis of hydrated ethylene glycol accounting for the antifreeze effect by using infrared attenuated total reflection spectroscopy, *J. Mol. Liq.*, 2016, **223**, 621–627.

42 R. Ishige, K. Tanaka and S. Ando, In Situ Analysis of Chain Orientation Behavior in Thin Film Aromatic Polyimides by Variable Temperature pMAIRS during Thermal Imidization, *Macromol. Chem. Phys.*, 2018, **219**, 1700370.

43 Z. Peng, L. Ye and H. Ade, Understanding, quantifying, and controlling the molecular ordering of semiconducting polymers: From novices to experts and amorphous to perfect crystals, *Mater. Horiz.*, 2022, **9**, 577–606.

44 S. A. Mollinger, B. A. Krajina, R. Noriega, A. Salleo and A. J. Spakowitz, Percolation, Tie-Molecules, and the Microstructural Determinants of Charge Transport in Semicrystalline Conjugated Polymers, *ACS Macro Lett.*, 2015, **4**, 708–712.

45 X. Li, P. J. Wolanin, L. R. MacFarlane, R. L. Harniman, J. Qian, O. E. C. Gould, T. G. Dane, J. Rudin, M. J. Cryan,

Open Access Article. Published on 20 January 2026. Downloaded on 6/13/2026 12:19:35 AM.
This article is licensed under a Creative Commons Attribution-NonCommercial 3.0 Unported Licence.

T. Schmaltz, H. Frauenrath, M. A. Winnik, C. F. J. Faul and I. Manners, Uniform electroactive fibre-like micelle nanowires for organic electronics, *Nat. Commun.*, 2017, **8**, 15909.

46 R. Qi, Y. Zhu, L. Han, M. Wang and F. He, Rectangular Platelet Micelles with Controlled Aspect Ratio by Hierarchical Self-Assembly of Poly(3-hexylthiophene)-b-poly(ethylene glycol), *Macromolecules*, 2020, **53**, 6555–6565.

47 Y. N. Pan, C. C. Ye, S. L. Huang, C. Wang, M. Y. Han and L. Xu, Precisely Prepared Hierarchical Micelles of Polyfluorene-block-Polythiophene-block-Poly(phenyl isocyanide) via Crystallization-Driven Self-Assembly, *Angew. Chem., Int. Ed.*, 2025, **64**, e202418131.

48 F. Niefind, S. Karande, F. Frost, B. Abel and A. Kahnt, Solvent influence on the surface morphology of P3HT thin films revealed by photoemission electron microscopy, *Nanoscale Adv.*, 2019, **1**, 3883–3886.

© 2026 The Author(s). Published by the Royal Society of Chemistry